JSHC
Japan Society of
Histochemistry and Cytochemistry
Established 1959

Acta Histochem. Cytochem. 51 (3): 101–110, 2018
doi: 10.1267/ahc.18019

Review

Label-free Molecular Imaging and Analysis by Raman Spectroscopy

Yasuaki Kumamoto[1], Yoshinori Harada[1], Tetsuro Takamatsu[2] and Hideo Tanaka[1]

[1]Department of Pathology and Cell Regulation, Graduate School of Medical Sciences, Kyoto Prefectural University of Medicine, 465 Kajii-cho, Kawaramachi-Hirokoji, Kamigyo-ku, Kyoto 602–8566, Japan and [2]Department of Medical Photonics, Kyoto Prefectural University of Medicine, 465 Kajii-cho, Kawaramachi-Hirokoji, Kamigyo-ku, Kyoto 602–8566, Japan

Received May 2, 2018; accepted May 25, 2018; published online June 20, 2018

Raman scattering of a cell conveys the intrinsic information inherent to chemical structures of biomolecules. The spectroscopy of Raman scattering, or Raman spectroscopy, allows label-free and quantitative molecular sensing of a biological sample *in situ* without disruption. For the last five decades Raman spectroscopy has been widely utilized in biological research fields. However, it is just within the latest decade that molecular imaging and discrimination of living cells and tissues have become practically available. Here we overview recent progress in Raman spectroscopy and its application to life sciences. We discuss imaging of functional molecules in living cells and tissues; e.g., cancer cells and ischemic or infarcted hearts, together with a number of studies in the biomedical fields. We further explore comprehensive understandings of a complex spectrum by multivariate analysis for, e.g., accurate peripheral nerve detection, and characterization of the histological differences in the healing process of myocardial infarct. Although limitations still remain, e.g., weakness of the scattering intensity and practical difficulty in comprehensive molecular analysis, continuous progress in related technologies will allow wider use of Raman spectroscopy for biomedical applications.

Key words: Raman scattering, spectroscopy, molecular imaging, label-free, multivariate analysis

I. Introduction

When a molecular substance is irradiated with light of a single wavelength (λ_i), light of different wavelengths (λ_s = λ_{s1}, λ_{s2}, ….) is scattered from the substance. Raman and Krishnan reported in 1928 that the wavelength shift of the inelastic scattering light ($\lambda_s \neq \lambda_i$) from the incident light corresponds to the energy of a molecular vibration [95]. This inelastic component is Raman scattering light. Figure 1A and 1B depicts the schematic representation of Raman scattering light and its spectrum, respectively. A spectrum of the scattering, in short a Raman spectrum, is inherent to a molecule. This is because vibrational modes of a molecule are determined by the chemical structure of the molecule. This Raman spectral inherency to a molecule can be understood from Fig. 1C, which represents the spectra of several biomolecules. Due to the molecular inherency, Raman spectra are used as intrinsic markers of specific molecules contained in cells and tissues. A Raman spectrum is often called “molecular fingerprint.”

The spectroscopy of Raman scattering, namely Raman spectroscopy, has several advantages over other methods in the study of life sciences. The most important one is that Raman spectroscopy does not require any particular pre-treatment; the spectral measurement of the living cell and tissue can be performed under a label-free condition. Labeling molecules used in the histochemical methods,

Correspondence to: Yasuaki Kumamoto and Hideo Tanaka, Department of Pathology and Cell Regulation, Graduate School of Medical Sciences, Kyoto Prefectural University of Medicine, 465 Kajii-cho, Kawaramachi-Hirokoji, Kamigyo-ku, Kyoto 602–8566, Japan.
E-mail: kumakpum@koto.kpu-m.ac.jp (Yasuaki Kumamoto) and hideotan@koto.kpu-m.ac.jp (Hideo Tanaka)

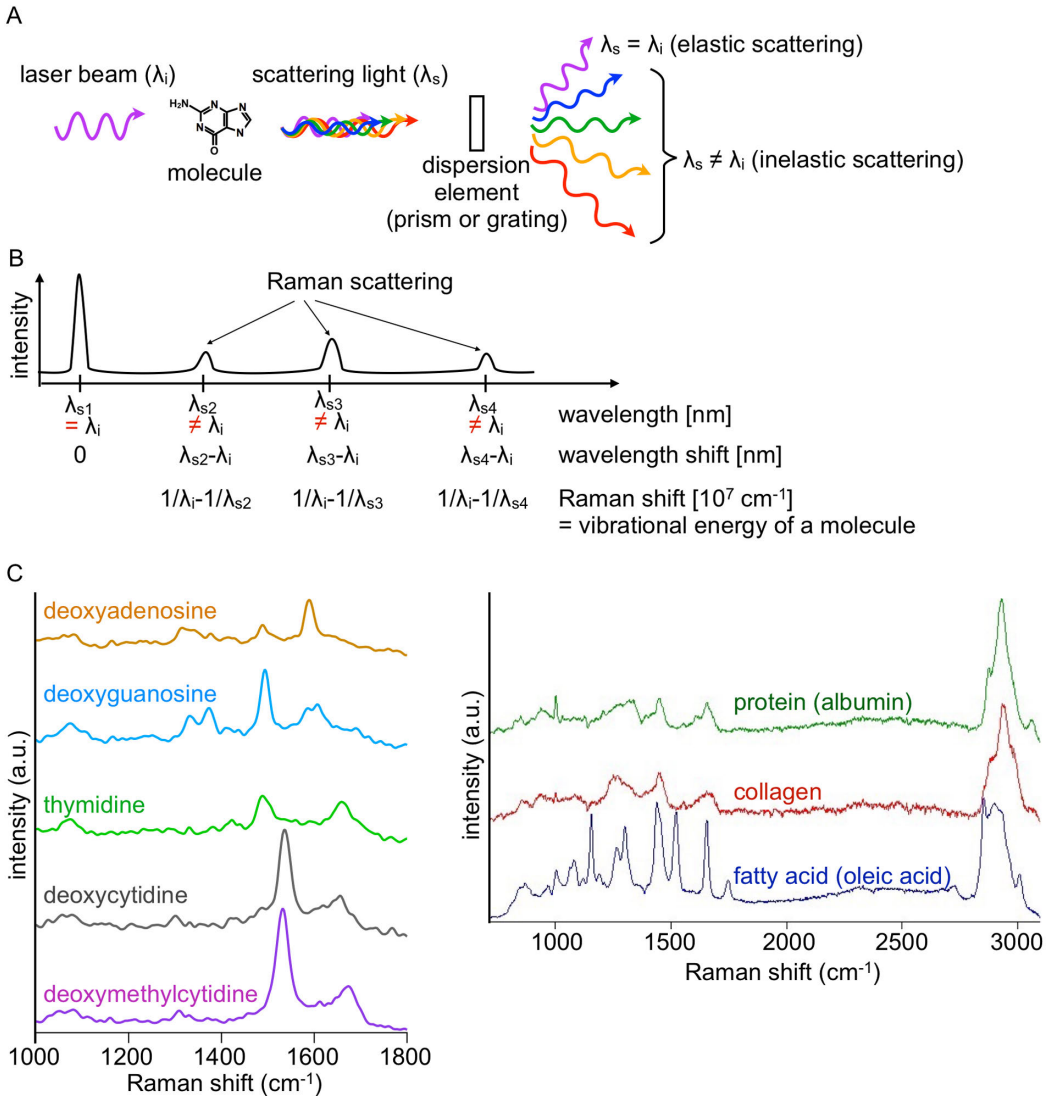

Fig. 1. **A**) An overview of light scattering by a molecule. Light scattered by a molecule contains elastic ($\lambda_s = \lambda_i$) and inelastic ($\lambda_s \neq \lambda_i$) components. **B**) A schematic representation of the relationship between wavelength shift of Raman scattering and vibrational energy of a molecule in a scattering spectrum. **C**) Raman spectra of biomolecules. λ_i: wavelength of incident light. λ_s, λ_{s1}, λ_{s2}, λ_{s3}, λ_{s4}: wavelengths of scattering light. a. u., arbitrary units.

such as fluorescent proteins and dyes, can modulate functions of a target molecule and states of living cells and tissues due to physical and/or chemical interaction. Second, a measurement target is not disrupted through measurement, unlike other label-free spectroscopy, such as mass spectrometry and laser-induced breakdown spectroscopy, both of which are accomplished by molecular ionization. Raman spectroscopy allows time-lapse analysis of the molecular dynamics of a living cell. Third, the measurement can be performed under any sample environment, e.g., liquid, air or vacuum. Finally, Raman spectroscopy reproduces quantitative information with high accuracy. The scattering intensity is proportional to the number of scatterers. Experimental errors along with erroneous or improper nonspecific labeling, disturbing quantitative measurement, do not show up in the measurement of Raman spectroscopy. A quantitative molecular measurement is also implementable for cells and tissues, composed of various molecules, when a comprehensive Raman spectral database of the molecules is available.

Thus, Raman spectroscopy allows label-free, non-disruptive, and quantitative molecular measurement and identification of biological samples *in situ*. Raman spectroscopy overcomes limitations of the histochemical methodologies to pave a new way in the life sciences. In this article, we overview the brief history of and recent topics in Raman spectroscopy in the life sciences. Potential usefulness, limitations and future outlooks are also discussed.

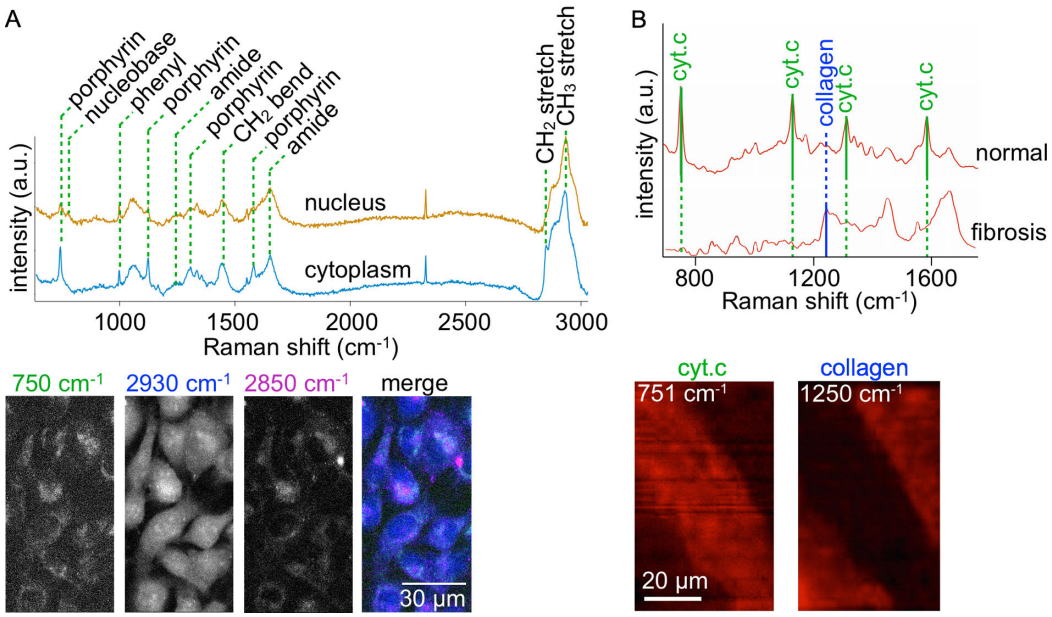

Fig. 2. **A**) Raman spectra and the band-specific images of 8505C cells. Major assignments of remarkable bands are shown in the upper panel. The lower panel shows four images reconstructed by the porphyrin ring (750 cm^{-1}), CH_3 (2930 cm^{-1}), and CH_2 (2850 cm^{-1}) bands, and a merge of the three images. The color channels of the merged image are assigned to 750 cm^{-1} (Green), 2930 cm^{-1} (Blue), and 2850 cm^{-1} (Magenta). **B**) Raman spectra of normal and fibrotic tissues of a rat myocardial infarct (upper panel). Cytochrome c (cyt. c) and collagen type I (collagen) bands are indicated in the spectra. The lower panel shows Raman images reconstructed with the collagen band of 1250 cm^{-1} and the cyt. c band of 751 cm^{-1}. Note that viable myocytes including cyt c show red signals, whereas fibrotic scar region is absent in the red signals. a. u., arbitrary units.

II. Brief History of Raman Spectroscopy

It was the year 1930 when Sir Raman was awarded the Nobel Prize in Physics for the discovery of Raman scattering. However, Raman scattering measurement had not been widely implemented until the late 1960s due to the lack of appropriate technologies, e.g., lasers, spectrographs, and detectors [42, 53, 86, 88]. Since the late 1960s, Raman scattering of a variety of biological constituents has been measured, and consequently spectral databases have been accumulated for nucleotides [2, 30, 69, 92, 96, 109, 110], peptides [17, 54, 70, 103, 104, 108], lipids [32, 63, 67, 68, 102, 113], and other components including apatites [11, 84], fibrils [33, 115], and pigments [35, 71, 74, 97, 98]. In the 1970s and later, Raman spectroscopy came to unveil molecular compositions in living cells [26, 80, 94] and biological tissues, such as bones [114, 115], teeth [78, 99], nerves [65, 89, 106], muscles [90, 91], arteries [7, 16, 25], eyes [36, 118], blood [8, 9, 64], and urine [93].

After the long period of early efforts, biomedical research by Raman spectroscopy has provided deeper insights into comprehensive molecular behaviors of living cells and tissues *in situ* under label-free, non-disruptive conditions. The details of these advances are described in the following sections.

III. Molecular Imaging

The spatial distribution of specific molecules is one of the most important pieces of information about living cells and tissues. However, the procedure of Raman spectral imaging (i.e., repetitive single spectral acquisitions with a detector array by two- or three-dimensional scan in space) takes a long time, 1 hour or longer per image. For acquisition of a spectral image within a short duration, it often occurs that the signal-to-noise ratio (S/N) and spatial resolution are low and the field of view is narrow. Although in the late 20th century fast Raman imaging modalities [13, 28, 34, 41, 72, 116, 120] were developed, they needed further advancements for biomedical applications. In those days, Raman spectral imaging was not put in practice because the properties of optical components (i.e., laser light sources, detectors, and filters) were inferior to those used today.

Raman spectral imaging has become practically useful for molecular analysis of living cells and tissues in the 21st century. A variety of molecules have been studied in different cells and tissues [4, 12, 22, 38, 47, 52, 58, 59, 60, 62, 87, 100, 111, 112]. Examples are shown in Fig. 2.

In Fig. 2A, shown are the nucleus and cytoplasm spectra of an 8505C cell line that were derived from human thyroid cancer, and the corresponding images reconstructed with the intensity at several wavenumbers. In the spectra, nine remarkable bands are identified, assigned to porphyrin

ring (750, 1127, 1314, and 1580 cm^{-1}), phenyl ring (1000 cm^{-1}), polypeptide (1250 and 1660 cm^{-1}), CH_2 (2850 cm^{-1}) and CH_3 (2930 cm^{-1}). According to a study [37], the porphyrin ring, CH_2, and CH_3 bands of living cultured cells are assigned to cytochrome c, lipid, and protein, respectively. In the image reconstructed with the porphyrin ring (750 cm^{-1}), the distributions of mitochondria are identified. The image of the CH_3 band shows the intracellular distributions of proteins. Intracellular distributions of vesicles and organelles are indicated in the image of the CH_2 band, assigned to lipid.

In the Raman data of a rat infarcted heart (Fig. 2B), the cytochrome c bands (i.e., mainly 751 cm^{-1}) are identified in the spectrum obtained from the non-infarcted (normal) region, while not in that of the infarcted (fibrosis) region. In contrast, the collagen band (i.e., 1250 cm^{-1}) is clearly seen in the spectrum of the fibrotic tissue, but not in that of the normal region. The corresponding images reconstructed with these two bands clearly reflect the two different patterns of the heart with infarction. Thus, Raman spectral imaging can discriminate myocardial infarct in a label-free manner.

Raman spectroscopy also allows study of dynamics of functional molecules of living cells. Time-lapse Raman spectral imaging has enabled us to understand a variety of molecular dynamics in cell functions, e.g., cell death processes [77, 83, 119], cell cycles [37, 43, 56, 57], endocytosis and intracellular transport [3, 6, 44], and differentiation [39]. Okada and his colleagues successfully performed label-free imaging of molecular dynamics in HeLa cells during development of apoptosis [83]. By using a slit-scan Raman microscope with a parallel spectral acquisition technique, they demonstrated that the application of actinomycin D clearly showed diffusion of cytochrome c from mitochondria to the cytosol in HeLa cells. Time-lapse, slit-scan Raman spectral imaging was also used for monitoring the process of osteoblast differentiation [39]. By Raman spectral imaging of KUSA-A1 cells (every 4 hours for 24 hours), it was found that β-carotene acts as an initial marker of osteoblastic mineralization that was monitored through hydroxyapatite. Temporal fluctuation of cytochrome c signals was also observed during mineralization, indicating that some of the cells measured underwent apoptosis. Similarly, Kong and his colleagues showed a potential usefulness of multifocal Raman microscopy, another parallel spectral acquisition technique [56, 57]. They successfully captured Ca^{2+}-dipicolinic acid (CaDPA), protein, and nucleic acid dynamics in a single Bacillus cereus spore during germination.

The above-mentioned fast Raman spectral imaging techniques have a limitation in terms of temporal resolution. Since a single spectral acquisition typically takes 10 ms or longer, longer than 1 min is required for acquisition of a typical Raman imaging dataset consisting of 10^4–10^5 spectra. Contrarily, the coherent Raman scattering processes, including stimulated Raman scattering (SRS) and coherent anti-Stokes Raman scattering (CARS), have enabled video-rate (30 frames per second) or faster Raman imaging. In a coherent Raman process, Raman scattering from target molecules is simultaneously excited by intense incident light so that the number of scattering photons in a short duration (e.g., microseconds) increases. Coherent Raman imaging techniques are useful for the analysis of rapid molecular dynamics, rapidly moving objects, and a vast number of samples. Limitations are that the coherent imaging techniques quickly degrade a sample because of the high incident photon density, and that the spectral resolution is low and the range of the spectrum is narrow in tradeoff with the image acquisition speed. A number of excellent comprehensive review articles discussing SRS and CARS microscopy for biomolecular imaging have been published elsewhere [18, 21, 24, 40, 60, 66].

IV. Discrimination by Multivariate Analysis

It is often difficult to thoroughly understand Raman spectra of a cell or tissue, because the spectra are typically low in S/N and complex. In contrast, algorithms of multivariate analyses, which can enhance the visibility of features in a dataset, allow comprehensive interpretations of Raman spectra. With the improvement of the calculation powers of computers since the 1990s, multivariate analysis of Raman spectra has become widely available for label-free, non-disruptive, and molecule-based clustering of different cells and tissues.

Here we show two examples of tissue discrimination based on Raman spectroscopy and multivariate analysis. The first one is peripheral nerve detection. Nerve sparing and repair procedures are essential in surgery, but with the methodologies currently used, such as visual inspection by a surgeon and muscular motion by electrical stimulation of a motor nerve, it is difficult to accurately and safely detect nerve bundles during operation. Label-free, non-disruptive Raman spectroscopy is applicable to peripheral nerve detection. Our experimental data for rats are shown in Fig. 3. In the figure, Raman spectra of peripheral nerves, tissues visually resembling the nerves, and their adjunct tissues are presented [75]. The spectra of peripheral nerves, i.e., intercostal and vagus nerves, include characteristic bands at 1004, 1130, 1176, 1247, 1304, 1445, 1589, 1662, 2850, 2885, and 2932 cm^{-1} (indicated by arrowheads). These bands are assigned either to protein, lipid, and/or collagen. Since the peripheral nerve consists of nerve fibers, blood vessels, perineurium, and endoneurium, all of these constituents, e.g., protein, lipid, and collagen, are contained in the nerve spectra to some extent. Contrarily, in the spectra of tissues adjacent to the nerves, including skeletal muscle tissues and adipose tissues, and of tissues visually resembling peripheral nerves, such as fibrous connective tissues and blood vessels, are mostly assigned to a single major component either of protein, lipid, or collagen. It is worth indicating that the higher intensity bands at 2850 and

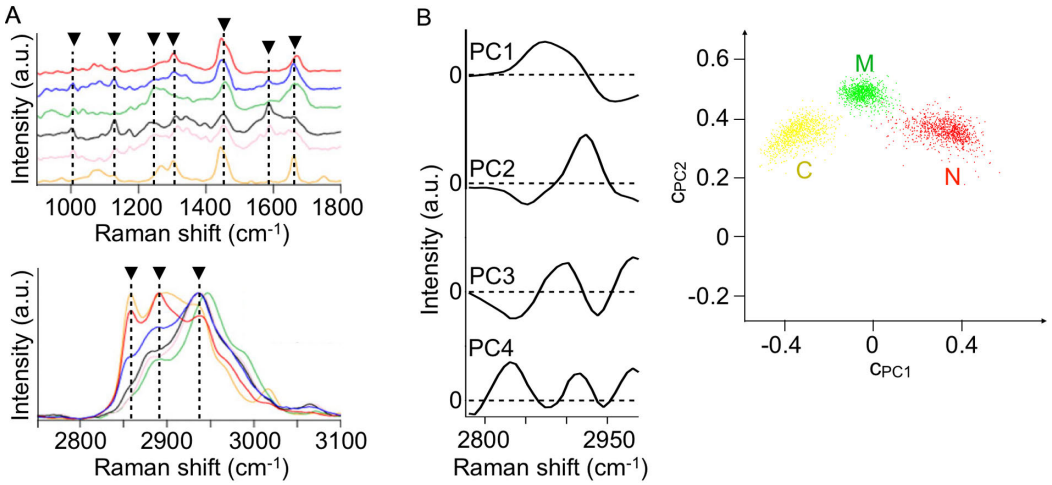

Fig. 3. **A**) Raman spectra of rat peripheral nerves, tissues visually resembling peripheral nerves, and their adjunct tissues. Two graphs showing different wavenumber ranges, 900–1800 cm^{-1} (upper) and 2750–3100 cm^{-1} (lower) are separately shown. Red: intercostal nerve. Blue: vagus nerve. Green: fibrous connective tissue. Black: blood vessel. Pink: skeletal muscle. Orange: adipose tissue. a. u., arbitrary units. Reproduced with permission from Ref 75. Copyright 2012 Springer-Verlag. **B**) A result of principal component regression analysis of the spectra of *ex vivo* rat sciatic, saphenous, and facial nerves, femoral skeletal muscle tissues, and connective tissues (leg tendons). The first to fourth principal components (PC1, PC2, PC3, and PC4) are shown on the left. The plots of the principal component coefficients to PC1 (c_{pc1}) and PC2 (c_{pc2}) for 3000 spectra are shown on the right. Red: peripheral nerve (n = 1000). Green: skeletal muscle (n = 1000). Yellow: connective tissue (n = 1000). C, connective tissue; M, skeletal muscle tissue; N, peripheral nerve. Reproduced from Ref 61.

2885 cm^{-1} in the intercostal nerve compared to in the vagus nerve reflect the larger amount of myelin sheath, which mainly consists of lipids, for the intercostal nerve because the nerves contain myelinated nerve fibers more abundantly than the vagus nerves do. Multivariate analysis of these spectra has provided accurate detection of nerve and non-nerve tissues [61, 76]. Results of principal component regression analysis of *ex vivo* rat tissue spectra are presented in Fig. 3B [61]. The accuracy of peripheral nerve detection against skeletal muscle and connective tissues is 99.6% [61], according to the discriminant analysis upon the data plot shown in Fig. 3B. It was also found that the discrimination of myelinated and unmyelinated nerves from adipose, fibrous connective, and skeletal muscle tissues is as accurate as 94.2% [76]. Aiming at clinical application of Raman spectroscopic nerve detection, rapid and accurate imaging of rat peripheral nerves was implemented by means of multipoint Raman spectroscopy and concurrent Raman and bright-field image data analyses [61].

The second example of tissue discrimination is the precise histological differences in the healing process of myocardial infarct. Fig. 4A shows Raman spectra of the infarct border zone during acute necrotizing, healing, and old fibrotic scar phases of infarcted rat heart [79]. Of great interest, the intensity of the 750 cm^{-1} band, assigned to cytochrome c, decreased during the progression of myocardial infarct; from the normal condition, via early (day 2) and late (day 5) necrosis phases, granulation tissue phase, and eventually the scar (fibrosis) phase. This tendency can be explained by the decrease in the number of living myocytes. Fibrotic tissues show remarkable bands assigned to collagen type I (1250 and 2941 cm^{-1}) in the spectra. Based on the spectral differences, partial least square discriminant analysis [79] and principal component analysis [81] could identify regions of distinct phases of myocardial infarct, i.e., intact, acute necrotizing, healing, and fibrotic tissues. Discrimination results and corresponding histological images are shown in Fig. 4B [79, 81]. In the principal component spectrum presented, the positive peaks at 751 m 1130, and 1582 cm^{-1}, assigned to cytochrome c, and the negative peaks at 857, 1250, and 2945 cm^{-1} notably reflect the totally opposite distributions of the normal and fibrotic tissues. According to the study [79], the accuracy of discrimination of the normal, necrosis, and granulation tissues was 95.8%. Recently, Ohira and his colleagues evaluated the early-stage ("nascent state") ischemic injury and the progressive evolution of the perfused rat heart evaluated by Raman spectroscopy [82]. It was found that 1) Raman bands of the redox states of cytochrome c (i.e., 750, 1127 cm^{-1}) increased immediately after stopping of coronary arterial flow, as shown in Fig. 4C, and 2) the cytochrome c signal can be a useful indicator for early ischemic injury of the heart.

Combination of Raman spectroscopy and multivariate analysis has also been employed for detection of a variety of diseased tissues, e.g., osteoarthritis [51], valvular heart disease [85], neoplasia in Barrett's oesophagus [50], and atherosclerosis [27].

Raman spectroscopy has also been applied to cancer and non-cancer discrimination. Excellent articles thoroughly reviewing this topic are published elsewhere [1, 5, 48, 55, 101]. Briefly, Raman spectroscopic cancer and non-cancer discrimination is in general based on a subtle change in overall molecular compositions due to the metabolic and

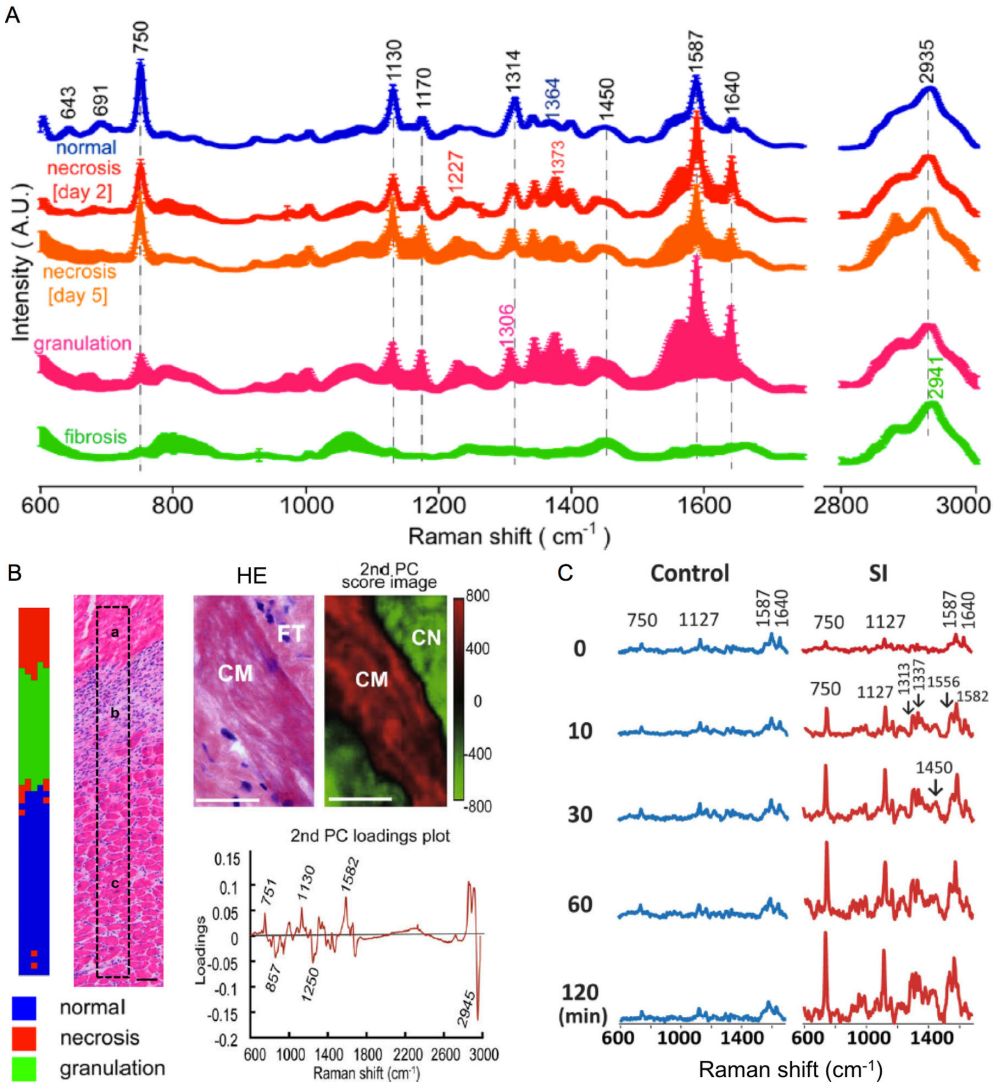

Fig. 4. **A**) Raman spectra of normal, necrotic, granulation, and fibrotic myocardial tissues of rats. Mean and mean ± standard deviations for individual spectral datasets are shown. A. U., arbitrary units. Reproduced with permission from Ref 79. Copyright 2014 American Chemical Society. **B**) Multivariate analysis results presenting marginal areas of injured myocardial tissues. Partial least square discriminant analysis classified the normal, necrosis, and granulation tissues, as validated by a hematoxylin and eosin (HE) image (left). Reproduced with permission from Ref 79. Copyright 2014 American Chemical Society. The second principal component classified the normal and fibrotic tissues, as validated by an HE image (right). Bars = 50 μm (left) and 20 μm (right). CM, cardiomyocyte; FT, fibrotic tissue; CN, collagen. Reproduced with permission from Ref 81. Copyright 2009 Elsevier Inc. **C**) Raman spectral evolution of early-state ischemic injury in the perfused rat heart. Raman bands of the redox states of cytochrome c (i.e., 750, 1127 cm^{-1}) increased immediately after ischemia started (30 min or less). Control: no ischemia. SI, simple ischemia; Reproduced from Ref 82.

morphological modifications in cancer, but no definitive marker specific for cancer is identified in a spectrum. Nevertheless, the accuracy of neoplastic and non-neoplastic tissue discrimination by Raman spectroscopy often exceeds 90% [10]. Taking advantage of the label-free and non-disruptive, and quantitative features, researchers have been pursuing applications of Raman spectroscopy to endoscopy.

Different kinds of cells at different states can be classified by means of Raman spectroscopy and multivariate analysis [15, 20, 31, 46, 73, 105]. Label-free, non-disruptive, and minimally invasive classification of different kinds of cells is particularly essential for stem cell study and regenerative medicine application. The potential of Raman spectroscopy for classification of undifferentiated and differentiated stem cells has been presented in the literature [14, 19, 45, 107, 117].

V. Limitations

Raman spectroscopy has two principal limitations for study and application in the life sciences. First, the efficiency of the Raman scattering process is extremely low,

typically 14 orders of magnitude as low as the fluorescence process. Due to the low scattering efficiency, acquiring a number of Raman spectra often takes several tens of minutes or even hours. During such a long acquisition time, spatiotemporal alteration in molecular distribution and sequential degradation of a measurement target can occur. Although the above-mentioned advanced techniques, e.g., slit-scan, multifocal, and coherent Raman imaging, allow fast acquisition for time-lapse analysis of molecular dynamics, these techniques are not widely used in the biomedical field. Additionally, signals from molecules at the relatively low concentration in a measurement target are hard to detect due to signals from massively existing molecules. Second, Raman bands of different molecules within a sample often overlap in a spectrum measured. Particularly in cells and tissues composed of a variety of molecular components, Raman bands of molecules with the low scattering efficiency and/or of a small amount cannot be identified. This limitation in turn results in the difficulty of totally comprehensive molecular analysis of the living cell and tissue in practice.

VI. Conclusion

Raman spectroscopy allows label-free, non-disruptive, and quantitative molecular analysis of cells and tissues. Because of these unique features, which cannot be provided by conventional methodologies in the life sciences, Raman spectroscopy has enabled identification and quantification of the biomolecules and their functional analysis *in situ*. In considering the unique features, we believe that Raman spectroscopy is, in particular, a powerful analytical tool for evaluation of spatiotemporal molecular dynamics of living cells and identification of intact human tissues. In contrast, trace molecular analysis and tissue identification without a specific molecular band are often difficult according to the limitations discussed above. Upon wider use of Raman spectroscopy in the future, the limitations need to be overcome; high throughput optical elements, techniques for fast Raman spectral imaging, and multivariate analysis algorithms will overcome the limitations in part. Additionally, well-established techniques for Raman scattering enhancement [49], e.g., surface-enhanced Raman scattering [23] and resonance Raman scattering [29], would help measure intrinsically weak Raman scattering.

VII. Conflicts of Interest

Y. K received a research grant from Nakatani Foundation for advancement of measuring technologies in biomedical engineering, and travel grants from Nakatani Foundation for advancement of measuring technologies in biomedical engineering, and The Murata Science Foundation. T. T. received a research grant from Toray Engineering Co., Ltd.

VIII. Acknowledgments

This work was supported in part by Japan Science and Technology Agency (JST) Core Research for Evolutional Science and Technology (CREST) program for Development and application of intelligent measurement-analysis methods through coalition between measurement technologies and informatics, and a Grand-in-Aid for Scientific Research (C) (16K01366) from Japan Society of the Promotion of Science (JSPS).

IX. References

1. Abramczyk, H. and Brozek-Pluska, B. (2013) Raman imaging in biochemical and biomedical applications. Diagnosis and treatment of breast cancer. *Chem. Rev.* 113; 5766–5781.
2. Alyward, N. N. and Koenig, J. L. (1970) Raman spectra of poly(adenylic acid). *Macromolecules* 3; 590–596.
3. Ando, J., Fujita, K., Smith, N. I. and Kawata, S. (2011) Dynamic SERS imaging of cellular transport pathways with endocytosed gold nanoparticles. *Nano Lett.* 11; 5344–5348.
4. Arikan, S., Sands, H. S., Rodway, R. G. and Batchelder, D. N. (2002) Raman spectroscopy and imaging of beta-carotene in live corpus luteum cells. *Anim. Reprod. Sci.* 71; 249–266.
5. Austin, L. A., Osseiran, S. and Evans, C. L. (2016) Raman technologies in cancer diagnostics. *Analyst* 141; 476–503.
6. Bando, K., Smith, N. I., Ando, J., Fujita, K. and Kawata, S. (2015) Analysis of dynamic SERS spectra measured with a nanoparticle during intracellular transportation in 3D. *J. Opt.* 17; 114023.
7. Baraga, J. J., Feld, M. S. and Rava, R. P. (1992) In situ optical histochemistry of human artery using near infrared Fourier transform Raman spectroscopy. *Proc. Natl. Acad. Sci. U S A* 89; 3473–3477.
8. Berger, A. J., Itzkan, I. and Feld, M. S. (1997) Feasibility of measuring blood glucose concentration by near-infrared Raman spectroscopy. *Spectrochim. Acta A* 53; 287–292.
9. Berger, A. J., Koo, T. W., Itzkan, I., Horowitz, G. and Feld, M. S. (1999) Multicomponent blood analysis by near-infrared Raman spectroscopy. *Appl. Opt.* 38; 2916–2926.
10. Berghold, M. S., Zheng, W., Lin, K., Ho, K. Y., Teh, M., Yeoh, K. G., So, J. B. Y. and Huang, Z. (2011) In vivo diagnosis of gastric cancer using Raman endoscopy and ant colony optimization techniques. *Int. J. Cancer* 128; 2673–2680.
11. Blakeslee, K. C. and Condrate, R. A. Sr. (1971) Vibrational spectra of hydrothermally prepared hydroxyapatites. *J. Am. Ceram. Soc.* 54; 559–563.
12. Bonetti, A., Bonifacio, A., Della Mora, A., Livi, U., Marchini, M. and Ortolani, F. (2015) Carotenoids co-localize with hydroxyapatite, cholesterol, and other lipids in calcified stenotic aortic valves. Ex vivo Raman maps compared to histological patterns. *Eur. J. Histochem.* 59; 93–97.
13. Bowden, M., Gardiner, D. J., Rice, G. and Gerrard, D. L. (1990) Line-scanned micro Raman spectroscopy using a cooled CCD imaging detector. *J. Raman Spectrosc.* 21; 37–41.
14. Brauchle, E., Knopf, A., Bauer, H., Shen, N., Linder, S., Monaghan, M. G., Ellwanger, K., Layland, S. L., Brucker, S. Y., Nsair, A. and Schenke-Layland, K. (2016) Non-invasive chamber-specific identification of cardiomyocytes in differentiating pluripotent stem cells. *Stem Cell Reports* 6; 188–199.
15. Brauchle, E., Thube, S., Brucker, S. Y. and Schenke-Layland, K. (2014) Cell death stages in single apoptotic and necrotic cells monitored by Raman microspectroscopy. *Sci. Rep.* 4; 4698.

16. Brennan, J. F. 3rd, Römer, T. J., Lees, R. S., Tercyak, A. M., Kramer, J. R. Jr. and Feld, M. S. (1997) Determination of human coronary artery composition by Raman spectroscopy. *Circulation* 96; 99–105.
17. Brunner, H. and Sussner, H. (1972) Raman scattering of native and thermally denatured lysozyme. *Biochim. Biophys. Acta* 271; 16–22.
18. Camp, C. H. Jr. and Cicerone, M. T. (2015) Chemically sensitive bioimaging with coherent Raman scattering. *Nat. Photonics* 9; 295–305.
19. Chan, J. W., Lieu, D. K., Huser, T. and Li, R. A. (2009) Label-free separation of human embryonic stem cells and their cardiac derivatives using Raman spectroscopy. *Anal. Chem.* 81; 1324–1331.
20. Chan, J. W., Taylor, D. S., Lane, S. M., Zwerdling, T., Tuscano, J. and Huser, T. (2008) Nondestructive identification of individual leukemia cells by laser trapping Raman spectroscopy. *Anal. Chem.* 80; 2180–2187.
21. Cheng, J. X. and Xie, X. S. (2015) Vibrational spectroscopic imaging of living systems: An emerging platform for biology and medicine. *Science* 350; aaa8870.
22. Chernenko, T., Sawant, R. R., Miljkovic, M., Quintero, L., Diem, M. and Torchilin, V. (2012) Raman microscopy for noninvasive imaging of pharmaceutical nanocarriers: intracellular distribution of cationic liposomes of different composition. *Mol. Pharm.* 9; 930–936.
23. Cialla-May, D., Zheng, X. S., Weber, K. and Popp, J. (2017) Recent progress in surface-enhanced Raman spectroscopy for biological and biomedical applications: from cells to clinics. *Chem. Soc. Rev.* 46; 3945–3961.
24. Cicerone, M. T. and Camp, C. H. Jr. (2018) Histological coherent Raman imaging: a prognostic review. *Analyst* 143; 33–59.
25. Clarke, R. H., Hanlon, E. B., Isner, J. M. and Brody, H. (1987) Laser Raman spectroscopy of calcified atherosclerotic lesions in cardiovascular tissue. *Appl. Opt.* 26; 3175–3177.
26. Dalterio, R. A., Nelson, W. H., Britt, D. and Sperry, J. F. (1987) An ultraviolet (242 nm excitation) resonance Raman study of live bacteria and bacterial components. *Appl. Spectrosc.* 41; 417–422.
27. Deinum, G., Rodriguez, D., Romer, T. J., Fitzmaurice, M., Kramer, J. R. and Feld, M. S. (1999) Histological classification of Raman spectra of human coronary artery atherosclerosis using principal component analysis. *Appl. Spectrosc.* 53; 938–942.
28. Duncan, M. D., Reintjes, J. and Manuccia, T. J. (1982) Scanning coherent anti-Stokes Raman microscope. *Opt. Lett.* 7; 350–352.
29. Efremov, E. V., Ariese, F. and Gooijer, C. (2008) Achievements in resonance Raman spectroscopy: Review of a technique with a distinct analytical chemistry potential. *Anal. Chim. Acta* 606; 119–134.
30. Erfurth, S. C., Kiser, E. J. and Peticolas, W. L. (1972) Determination of the backbone structure of nucleic acids and nucleic acid oligomers by laser Raman scattering. *Proc. Natl. Acad. Sci. U S A* 69; 938–941.
31. Escoriza, M. F., Van Briesen, J. M., Stewart, S. and Maier, J. (2007) Raman spectroscopic discrimination of cell response to chemical and physical inactivation. *Appl. Spectrosc.* 61; 812–823.
32. Forrest, G. (1978) Raman spectroscopy of the milk globule membrane and triglycerides. *Chem. Phys. Lipids* 21; 237–252.
33. Frushour, B. G. and Koenig, J. L. (1975) Raman scattering of collagen, gelatin, elastin. *Biopolymers* 14; 379–391.
34. Gift, A. D., Ma, J., Haber, K. S., McClain, B. L. and Ben-Amotz, D. (1999) Near-infrared Raman imaging microscope based on fiber-bundle image compression. *J. Raman Spectrosc.* 30; 757–765.
35. Gill, D., Kilponen, R. G. and Rimai, L. (1970) Resonance Raman scattering of laser radiation by vibrational modes of carotenoid pigment molecules in intact plant tissues. *Nature* 227; 743–744.
36. Goheen, S. C., Lis, L. J. and Kauffman, J. W. (1978) Raman spectroscopy of intact feline corneal collagen. *Biochim. Biophys. Acta* 536; 197–204.
37. Hamada, K., Fujita, K., Smith, N. I., Kobayashi, M., Inouye, Y. and Kawata, S. (2008) Raman microscopy for dynamic molecular imaging of living cells. *J. Biomed. Opt.* 13; 044027.
38. Harada, Y. and Takamatsu, T. (2013) Raman molecular imaging of cells and tissues: towards functional diagnostic imaging without labeling. *Curr. Pharm. Biotechnol.* 14; 133–140.
39. Hashimoto, A., Yamaguchi, Y., Chiu, L. D., Morimoto, C., Fujita, K., Takedachi, M., Kawata, S., Murakami, S. and Tamiya, E. (2015) Time-lapse Raman imaging of osteoblast differentiation. *Sci. Rep.* 5; 12529.
40. Hashimoto, M. (2002) Coherent anti-Stokes Raman scattering microscopy. *Acta Histochem. Cytochem.* 35; 83–86.
41. Hashimoto, M., Araki, T. and Kawata, S. (2000) Molecular vibration imaging in the fingerprint region by use of coherent anti-Stokes Raman scattering microscopy with a collinear configuration. *Opt. Lett.* 25; 1768–1770.
42. Hendra, P. J. and Stratton, P. M. (1969) Laser-Raman spectroscopy. *Chem. Rev.* 69; 325–344.
43. Huang, C. K., Hamaguchi, H. O. and Shigeto, S. (2011) In vivo multimode Raman imaging reveals concerted molecular composition and distribution changes during yeast cell cycle. *Chem. Commun.* 47; 9423–9425.
44. Huang, K. C., Bando, K., Ando, J., Smith, N. I., Fujita, K. and Kawata, S. (2014) 3D SERS (surface-enhanced Raman scattering) imaging of intracellular pathways. *Methods* 68; 348–353.
45. Ichimura, T., Chiu, L. D., Fujita, K., Kawata, S., Watanabe, T. M., Yanagida, T. and Fujita, H. (2014) Visualizing cell state transition using Raman spectroscopy. *PLoS One* 9; e84478.
46. Jarvis, R. M. and Goodacre, R. (2004) Ultra-violet resonance Raman spectroscopy for the rapid discrimination of urinary tract infection bacteria. *FEMS Microbiol. Lett.* 232; 127–132.
47. Kann, B., Offerhaus, H. L., Windbergs, M. and Otto, C. (2015) Raman microscopy for cellular investigations—From single cell imaging to drug carrier uptake visualization. *Adv. Drug Deliv. Rev.* 89; 71–90.
48. Kast, R. E., Tucker, S. C., Killian, K., Trexler, M., Honn, K. V. and Auner, G. W. (2014) Emerging technology: Applications of Raman spectroscopy for prostate cancer. *Cancer Metastasis Rev.* 33; 673–693.
49. Kawata, S., Ichimura, T., Taguchi, A. and Kumamoto, Y. (2017) Nano-Raman scattering microscopy: Resolution and enhancement. *Chem. Rev.* 117; 4983–5001.
50. Kendall, C., Stone, N., Shepherd, N., Geboes, K., Warren, B., Bennett, R. and Barr, H. (2003) Raman spectroscopy, a potential tool for the objective identification and classification of neoplasia in Barrett's oesophagus. *J. Pathol.* 200; 602–609.
51. Kerns, J. G., Gikas, P. D., Buckley, K., Sheppard, A., Birch, H. L., McCarthy, I., Miles, J., Briggs, T. W. R., Keen, R., Parker, A. W., Matousek, P. and Goodship, A. E. (2014) Evidence from Raman spectroscopy of a putative link between inherent bone matrix chemistry and degenerative joint disease. *Arthritis Rheumatol.* 66; 1237–1246.
52. Kochan, K., Maslak, E., Krafft, C., Kostogrys, R., Chlopicki, S. and Baranska, M. (2015) Raman spectroscopy analysis of lipid droplets content, distribution and saturation level in Non-Alcoholic Fatty Liver Disease in mice. *J. Biophotonics* 8; 597–609.
53. Koenig, J. L. (1972) Raman spectroscopy of biological molecules: A review. *J. Polym. Sci. D* 6; 59–177.

54. Koenig, J. L. and Sutton, P. L. (1969) Raman spectrum of the right-handed α-helix of poly-L-alanine. *Biopolymers* 8; 167–171.
55. Kong, K., Kendall, C., Stone, N. and Notingher, I. (2015) Raman spectroscopy for medical diagnostics—From in-vitro biofluid assays to in-vivo cancer detection. *Adv. Drug Deliv. Rev.* 89; 121–134.
56. Kong, L., Setlow, P. and Li, Y. Q. (2014) Observation of the dynamic germination of single bacterial spores using rapid Raman imaging. *J. Biomed. Opt.* 19; 011003.
57. Kong, L., Zhang, P., Yu, J., Setlow, P. and Li, Y. Q. (2011) Rapid confocal Raman imaging using a synchro multifoci-scan scheme for dynamic monitoring of single living cells. *Appl. Phys. Lett.* 98; 213703.
58. Konorov, S. O., Schulze, H. G., Atkins, C. G., Piret, J. M., Aparicio, S. A., Turner, R. F. and Blades, M. W. (2011) Absolute quantification of intracellular glycogen content in human embryonic stem cells with Raman microspectroscopy. *Anal. Chem.* 83; 6254–6258.
59. Krafft, C., Knetschke, T., Funk, R. H. and Salzer, R. (2006) Studies on stress-induced changes at the subcellular level by Raman microspectroscopic mapping. *Anal. Chem.* 78; 4424–4429.
60. Krafft, C., Schmitt, M., Schie, I. W., Cialla-May, D., Matthäus, C., Bocklitz, T. and Popp, J. (2017) Label-free molecular imaging of biological cells and tissues by linear and nonlinear Raman spectroscopic approaches. *Angew. Chem. Int. Ed. Engl.* 56; 4392–4430.
61. Kumamoto, Y., Harada, Y., Tanaka, H. and Takamatsu, T. (2017) Rapid and accurate peripheral nerve imaging by multipoint Raman spectroscopy. *Sci. Rep.* 7; 845.
62. Kumamoto, Y., Taguchi, A., Smith, N. I. and Kawata, S. (2012) Deep ultraviolet resonant Raman imaging of a cell. *J. Biomed. Opt.* 17; 076001.
63. Larsson, K. (1973) Conformation-dependent features in the Raman spectra of simple lipids. *Chem. Phys. Lipids* 10; 165–176.
64. Larsson, K. and Hellgren, L. (1974) A study of the combined Raman and fluorescence scattering from human blood plasma. *Experientia* 30; 481–483.
65. Larsson, K. and Rand, R. P. (1973) Detection of changes in the environment of hydrocarbon chains by Raman spectroscopy and its application to lipid-protein systems. *Biochim. Biophys. Acta* 326; 245–255.
66. Lee, H. J. and Cheng, J. X. (2017) Imaging chemistry inside living cells by stimulated Raman scattering microscopy. *Methods* 128; 119–128.
67. Lippert, J. L. and Peticolas, W. L. (1971) Laser Raman investigation of the effect of cholesterol on conformational changes in dipalmitoyl lecithin multilayers. *Proc. Natl. Acad. Sci. U S A* 68; 1572–1576.
68. Lippert, J. L. and Peticolas, W. L. (1972) Raman active vibrations in long-chain fatty acids and phospholipid sonicates. *Biochim. Biophys. Acta* 282; 8–17.
69. Lord, R. C. and Thormas, G. J. Jr. (1967) Raman spectral studies of nucleic acids and related molecules–I Ribonucleic acid derivatives. *Spectrochim. Acta* 23; 2551–2591.
70. Lord, R. C. and Yu, N. T. (1970) Laser-excited Raman spectroscopy of biomolecules: I. Native lysozyme and its constituent amino acids. *J. Mol. Biol.* 50; 509–524.
71. Lutz, M. (1974) Resonance Raman spectra of chlorophyll in solution. *J. Raman Spectrosc.* 2; 497–516.
72. Ma, J. and Ben-Amotz, D. (1997) Rapid micro-Raman imaging using fiber-bundle image compression. *Appl. Spectrosc.* 51; 1845–1848.
73. Maquelin, K., Choo-Smith, L. P., van Vreeswijk, T., Endtz, H. P., Smith, B., Bennett, R., Bruining, H. A. and Puppels, G. J. (2000) Raman spectroscopic method for identification of clinically relevant microorganisms growing on solid culture medium. *Anal. Chem.* 72; 12–19.
74. Margulies, L. and Stockburger, M. (1979) Spectroscopic studies on model compounds of the phychrome chromophore. Protonation and deprotonation of biliverdin dimethyl ester. *J. Am. Chem. Soc.* 101; 743–744.
75. Minamikawa, T., Harada, Y., Koizumi, N., Okihara, K., Kamoi, K., Yanagisawa, A. and Takamatsu, T. (2013) Label-free detection of peripheral nerve tissues against adjacent tissues by spontaneous Raman microspectroscopy. *Histochem. Cell Biol.* 139; 181–193.
76. Minamikawa, T., Harada, Y. and Takamatsu, T. (2015) Ex vivo peripheral nerve detection of rats by spontaneous Raman spectroscopy. *Sci. Rep.* 5; 17165.
77. Naito, Y., Toh-e, A. and Hamaguchi, H. O. (2005) In vivo time-resolved Raman imaging of a spontaneous death process of a single budding yeast cell. *J. Raman Spectrosc.* 36; 837–839.
78. Nishigori, K., Yamashita, S. and Yamada, M. (1986) A biophysical study on characterization of fish teeth by Raman-microspectrometry and microfluorometry. *Acta Histochem. Cytochem.* 19; 277–287.
79. Nishiki-Muranishi, N., Harada, Y., Minamikawa, T., Yamaoka, Y., Dai, P., Yaku, H. and Takamatsu, T. (2014) Label-free evaluation of myocardial infarction and its repair by spontaneous Raman spectroscopy. *Anal. Chem.* 86; 6903–6910.
80. Nocentini, S. and Chinsky, L. (1983) In vivo studies of nucleic acid by ultraviolet resonance Raman spectroscopy on eukaryotic living cells. *J. Raman Spectrosc.* 14; 9–10.
81. Ogawa, M., Harada, Y., Yamaoka, Y., Fujita, K., Yaku, H. and Takamatsu, T. (2009) Label-free biochemical imaging of heart tissue with high-speed spontaneous Raman microscopy. *Biochem. Biophys. Res. Commun.* 382; 370–374.
82. Ohira, S., Tanaka, H., Harada, Y., Minamikawa, T., Kumamoto, Y., Matoba, S., Yaku, H. and Takamatsu, T. (2017) Label-free detection of myocardial ischaemia in the perfused rat heart by spontaneous Raman spectroscopy. *Sci. Rep.* 7; 42401.
83. Okada, M., Smith, N. I., Palonpon, A. F., Endo, H., Kawata, S., Sodeoka, M. and Fujita, K. (2012) Label-free Raman observation of cytochrome c dynamics during apoptosis. *Proc. Natl. Acad. Sci. U S A* 109; 28–32.
84. O'Shea, D. C., Bartlett, M. L. and Young, R. A. (1974) Compositional analysis of apatites with laser-Raman spectroscopy: (OH,F,Cl)apatites. *Arch. Oral Biol.* 19; 995–1006.
85. Otero, E. U., Sathaiah, S., Silveira, L. Jr., Pomerantzeff, P. M. A. and Pasqualucci, C. A. G. (2004) Raman spectroscopy for diagnosis of calcification in human heart valves. *Spectroscopy* 18; 75–84.
86. Ozaki, Y. (1988) Medical applications of Raman spectroscopy. *Appl. Spectrosc. Rev.* 24; 259–312.
87. Palonpon, A. F., Sodeoka, M. and Fujita, K. (2013) Molecular imaging of live cells by Raman microscopy. *Curr. Opin. Chem. Biol.* 17; 708–715.
88. Peticolas, W. L. (1975) Application of Raman spectroscopy to biological macromolecules. *Biochimie* 57; 417–428.
89. Pézolet, M. and Georgescauld, D. (1985) Raman spectroscopy of nerve fibers. A study of membrane lipids under steady state conditions. *Biophys. J.* 47; 367–372.
90. Pezolet, M., Pigeon-Gosselin, M. and Caille, J. P. (1978) Laser Raman investigations of intact single muscle fibers. Protein conformations. *Biochim. Biophys. Acta* 533; 263–269.
91. Pézolet, M., Pigeon-Gosselin, M., Nadeau, J. and Caillé, J. P. (1980) Laser Raman scattering. A molecular probe of the contractile state of intact single muscle fibers. *Biophys. J.* 31; 1–8.

92. Pézolet, M., Yu, T. J. and Peticolas, W. L. (1975) Resonance and preresonance Raman spectra of nucleotides using ultraviolet lasers. *J. Raman Spectrosc.* 3; 55–64.
93. Premasiri, W. R., Clarke, R. H. and Womble, M. E. (2001) Urine analysis by laser Raman spectroscopy. *Lasers Surg. Med.* 28; 330–334.
94. Puppels, G. J., De Mul, F. F. M., Otto, C., Greve, J., Robert-Nicoud, M., Arndt-Jovin, D. J. and Jovin, T. M. (1990) Studying single living cells and chromosomes by confocal Raman microspectroscopy. *Nature* 347; 301–303.
95. Raman, C. V. and Krishnan, K. S. (1928) A new type of secondary radiation. *Nature* 121; 501–502.
96. Rimai, L., Cole, T., Parsons, J. L., Hickmott, J. T. Jr. and Carew, E. B. (1969) Studies of Raman spectra of water solutions of adenosine tri-, di-, and monophosphate and some related compounds. *Biophys. J.* 9; 320–329.
97. Rimai, L., Gill, D. and Parsons, J. L. (1971) Raman spectra of dilute solutions of some stereoisomers of vitamin A type molecules. *J. Am. Chem. Soc.* 93; 1353–1357.
98. Rimai, L., Kilponen, R. G. and Gill, D. (1970) Resonance-enhanced Raman spectra of visual pigments in intact bovine retinas at low temperatures. *Biochem. Biophys. Res. Commun.* 41; 492–497.
99. Rippon, W. B., Koenig, J. L. and Walton, A. G. (1971) Laser Raman spectroscopy of biopolymers and proteins. *J. Agric. Food Chem.* 19; 692–697.
100. Sharifzadeh, M., Zhao, D. Y., Bernstein, P. S. and Gellermann, W. (2008) Resonance Raman imaging of macular pigment distributions in the human retina. *J. Opt. Soc. Am. A* 25; 947–957.
101. Singh, S. P., Ibrahim, O., Byrne, H. J., Mikkonen, J. W., Koistinen, A. P., Kullaa, A. M. and Lyng, F. M. (2016) Recent advances in optical diagnosis of oral cancers: Review and future perspectives. *Head Neck* 38; E2403–E2411.
102. Spiker, R. C. Jr. and Levin, I. W. (1975) Raman spectra and vibrational assignments for dipalmitoyl phosphatidylcholine and structurally related molecules. *Biochim. Biophys. Acta* 388; 361–373.
103. Spiro, T. G. and Strekas, T. C. (1972) Resonance Raman spectra of hemoglobin and cytochrome c: inverse polarization and vibronic scattering. *Proc. Natl. Acad. Sci. U S A* 69; 2622–2626.
104. Sugawara, Y., Harada, I., Matsuura, H. and Shimanouchi, T. (1978) Preresonance Raman studies of poly(L-lysine), poly(L-glutamic acid), and deuterated N-methylacetamides. *Biopolymers* 17; 1405–1421.
105. Swain, R. J., Jell, G. and Stevens, M. M. (2008) Non-invasive analysis of cell cycle dynamics in single living cells with Raman micro-spectroscopy. *J. Cell Biochem.* 104; 1427–1438.
106. Szalontai, B., Bagyinka, C. and Horváth, L. I. (1977) Changes in the Raman spectrum of frog sciatic nerve during action potential propagation. *Biochem. Biophys. Res. Commun.* 76; 660–665.
107. Tan, Y., Konorov, S. O., Schulze, H. G., Piret, J. M., Blades, M. W. and Turner, R. F. (2012) Comparative study using Raman microspectroscopy reveals spectral signatures of human induced pluripotent cells more closely resemble those from human embryonic stem cells than those from differentiated cells. *Analyst* 137; 4509–4515.
108. Tobin, M. C. (1968) Raman spectra of crystalline lysozyme, pepsin, and alpha chymotrypsin. *Science* 161; 68–69.
109. Tobin, M. C. (1969) The Raman spectra of calf thymus and of salmon testes deoxyribonucleic acid. *Spectrochim. Acta* 25; 1855–1864.
110. Tomlinson, B. L. and Peticolas, W. L. (1970) Conformational dependence of Raman scattering intensities in polyadenylic acid. *J. Chem. Phys.* 52; 2154–2156.
111. Uzunbajakava, N., Lenferink, A., Kraan, Y., Volokhina, E., Vrensen, G., Greve, J. and Otto, C. (2003) Nonresonant confocal Raman imaging of DNA and protein distribution in apoptotic cells. *Biophys. J.* 84; 3968–3981.
112. van Manen, H. J., Kraan, Y. M., Roos, D. and Otto, C. (2005) Single-cell Raman and fluorescence microscopy reveal the association of lipid bodies with phagosomes in leukocytes. *Proc. Natl. Acad. Sci. U S A* 102; 10159–10164.
113. Verma, S. P. and Wallach, D. F. H. (1977) Raman spectra of some saturated, unsaturated and deuterated C_{18} fatty acids in the HCH-deformation and CH-stretching regions. *Biochim. Biophys. Acta* 486; 217–227.
114. Walters, M. A., Leung, Y. C., Blumenthal, N. C., LeGeros, R. Z. and Konsker, K. A. (1990) A Raman and infrared spectroscopic investigation of biological hydroxyapatite. *J. Inorg. Biochem.* 39; 193–200.
115. Walton, A. G., Deveney, M. J. and Koenig, J. L. (1970) Raman spectroscopy of calcified tissue. *Calcif. Tissue Res.* 6; 162–167.
116. Watanabe, M. and Ogawa, T. (1988) Raman scattering and photoluminescence tomography. *Jpn. J. Appl. Phys.* 27; 1066–1070.
117. Wu, H. H., Ho, J. H. and Lee, O. K. (2016) Detection of hepatic maturation by Raman spectroscopy in mesenchymal stromal cells undergoing hepatic differentiation. *Stem Cell Res. Ther.* 7; 6.
118. Yu, N. T., Jo, B. H., Chang, R. C. C. and Huber, J. D. (1974) Single-crystal Raman spectra of native insulin structures of insulin fibrils, glucagon fibrils, and intact calf lens. *Arch. Biochem. Biophys.* 160; 614–622.
119. Zoladek, A., Pascut, F. C., Patel, P. and Notingher, I. (2011) Non-invasive time-course imaging of apoptotic cells by confocal Ramanmicro-spectroscopy. *J. Raman Spectrosc.* 42; 251–258.
120. Zumbusch, A., Holtom, G. R. and Xie, X. S. (1999) Three-dimensional vibrational imaging by coherent anti-Stokes Raman scattering. *Phys. Rev. Lett.* 82; 4142–4145.